Protein Science (1997), *6*:1016–1023. Cambridge University Press. Printed in the USA.

Identification of a novel bond between a histidine and the essential tyrosine in catalase HPII of *Escherichia coli*

JERONIMO BRAVO,[1,5] IGNACIO FITA,[1] JUAN C. FERRER,[2] WERNER ENS,[3] ALEX HILLAR,[4] JACEK SWITALA,[4] AND PETER C. LOEWEN[4]

[1]Centro de Investigación y Desarrollo (C.S.I.C.), Jordi Girona Salgado 18-26, 08034 Barcelona, Spain
[2]Departament de Bioquímica i Biologia Molecular, Facultat de Química, Universitat de Barcelona, Martí i Franquès 1, 08028 Barcelona, Spain
[3]Department of Physics, University of Manitoba, Winnipeg, MB R3T 2N2 Canada
[4]Department of Microbiology, University of Manitoba, Winnipeg, MB R3T 2N2 Canada

(RECEIVED December 16, 1996; ACCEPTED February 12, 1997)

Abstract

A bond between the N_δ of the imidazole ring of His 392 and the C_β of the essential Tyr 415 has been found in the refined crystal structure at 1.9 Å resolution of catalase HPII of *Escherichia coli*. This novel type of covalent linkage is clearly defined in the electron density map of HPII and is confirmed by matrix-assisted laser desorption/ionization mass spectrometry analysis of tryptic digest mixtures. The geometry of the bond is compatible with both the sp^3 hybridization of the C_β atom and the planarity of the imidazole ring. Two mutated variants of HPII active site residues, H128N and N201H, do not contain the His 392–Tyr 415 bond, and their crystal structures show that the imidazole ring of His 392 was rotated, in both cases, by 80° relative to its position in HPII. These mutant forms of HPII are catalytically inactive and do not convert heme *b* to heme *d*, suggesting a relationship between the self-catalyzed heme conversion reaction and the formation of the His-Tyr linkage. A model coupling the two processes and involving the reaction of one molecule of H_2O_2 on the proximal side of the heme with compound I is proposed.

Keywords: catalase; crystal structure; *Escherichia coli*; heme; histidine–tyrosine linkage; protein modification

Catalases have been the object of study for almost a century. They are produced by most aerobic organisms as protection against the toxic effects of H_2O_2, which is degraded to O_2 and H_2O in the reaction: $2H_2O_2 \rightarrow O_2 + 2H_2O$. The enzyme from bovine liver has been the focus of extensive physical and kinetic studies, culminating in its sequence analysis and crystal structure determination in the early 1980s as a homotetramer of 55-kDa subunits (Murthy et al., 1981; Fita et al., 1986). The three-dimensional structures of four other catalases have been solved, including enzymes from *Penicillium vitale* (Vainshtein et al., 1981, 1986), *Proteus mirabilis* (Gouet et al., 1995), *Micrococcus luteus* (Murshudov et al., 1992), and *Escherichia coli* (Bravo et al., 1995), revealing extensive structural similarities among all five proteins, not surprising in view of the high sequence similarity in the core of the subunit around the active site.

Despite the similarities in the core, *P. vitale* and *E. coli* catalases have much larger subunits of more than 80 kDa, and a different heme giving rise to additional structural features, enhanced stability, and peculiarities in the catalytic properties compared with the small subunit enzymes. The additional sequence is contained in extensions at the amino and carboxyl ends. In HPII of *E. coli*, 90 additional residues at the N-terminus interact extensively with an adjacent subunit to produce an unusually stable quaternary structure. The 170 additional residues at the carboxyl terminus are folded in a flavodoxin-like domain whose possible roles remain unknown (Bravo et al., 1995). Another relevant difference from the small subunit catalases lies in the presence of a *cis*-hydroxy spirolactone heme *d* that is "flipped" 180° around the axis defined by the α-γ meso carbon atoms, relative to the orientation of the heme *b* found in the smaller catalases (Murshudov et al., 1996). The oxidation of the heme in HPII is catalyzed by HPII itself, which uses H_2O_2 as substrate (Loewen et al., 1993). However, the modification occurs on the proximal side of ring III of the heme, at a significant distance from the catalytic residues, His 128 and Asn 201, and a satisfactory mechanism for the oxidation has yet to be proposed.

Another modification found in HPII involves the blockage of the sulfhydryl group of Cys 438, one of two cysteines in the protein. The modification, with a mass of 42, is sensitive to alkali, but not to hydroxylamine, methylamine, or reducing agents, eliminating many common sulfhydryl blocking groups (Sevinc et al., 1995) and, to date, remains undefined. Another unusual modifica-

Reprint requests to: Peter C. Loewen, Department of Microbiology, University of Manitoba, Winnipeg, MB R3T 2N2 Canada; e-mail: peter_loewen@umanitoba.ca.
[5]Present address: Laboratory of Molecular Biophysics, The Rex Richards Building, South Parks Road, Oxford OX1 3OU, United Kingdom.

tion has been characterized in the catalase from *P. mirabilis* where a methionine sulfone is found adjacent to the active site histidine, replacing the more common valine found in most other catalases (Buzy et al., 1995).

From these observations, it has become clear that catalases in general and HPII in particular contain a number of unusual structural modifications. The structure of HPII, at 1.9 Å resolution, and of two inactive variants, H128N at 1.9 Å and N201H at 2.2 Å, have been refined recently, and a detailed analysis of the structure is in progress currently. This paper describes the identification of another novel modification, a histidine–tyrosine linkage, that is present in HPII, but not in the inactive H128N and N201H variants. This modification was not evident in the earlier analysis (Bravo et al., 1995) at the lower resolution, 2.8 Å, then available.

Results

HPII crystal structure reveals a novel His-Tyr association

In performing the refinement of the structure of native catalase HPII, the electron density maps revealed that the imidazole ring of His 392 had a strong tendency to be situated in close contact to Tyr 415, the tyrosinate fifth ligand of the heme iron, despite the restraints imposed by steric repulsion. When the nonbonded contacts between His 392 and Tyr 415 were not included in the refinement, the imidazole ring was oriented such that its N_δ was located less than 1.6 Å from the C_β of Tyr 415 in the four crystallographically independent HPII subunits (Fig. 1A). This distance is, within experimental error, what is expected for a C-N covalent bond (1.48 Å; MacGillavry & Rieck, 1968), and precludes a noncovalent interaction. The $2F_o - F_c$ and omit maps reveal a clear connection between His 392 and Tyr 415 (Fig. 1B), with an electron density as strong as any other covalent bond along the main chain, suggesting that the bond exists in a high proportion, close to 100%, of the subunits. Furthermore, the orientation of the imidazole ring is defined very clearly by the presence of a water molecule that forms a linear hydrogen bond, distance 2.8 Å, with the N_ϵ-atom of the imidazole (Fig. 1A). The geometry of this novel His-Tyr bond is compatible with both the sp^3 hybridization of the Tyr 415-C_β atom and the planarity of the imidazole ring, which makes a dihedral angle of 69° with the plane defined by the C_α-C_β-C_γ atoms of Tyr 415.

By contrast, the electron density maps corresponding to H128N and N201H, two mutated inactive variants of HPII, show a clear separation of the imidazole ring of His 392 from Tyr 415, a result of rotation of the imidazole ring by about 80° compared to its location in HPII. Results for H128N are given in Figure 1C. This rotation moves the N_δ to a point 3.5 Å away from C_β of Tyr 415, precluding any possible association between the two atoms.

Analysis of tryptic peptides by matrix-assisted laser desorption/ionization mass spectrometry (MALDI-MS)

In order to corroborate the presence of the novel C-N linkage between His 392 and Tyr 415, the peptides generated by trypsin digestion were subjected to mass analysis using MALDI-MS. Complete digestion of HPII by trypsin should generate a mixture of 75 peptide products, which will be further complicated, particularly below 3,000 mass units, by the presence of partial digest products. His 392 and Tyr 415 are situated on separate but adjacent tryptic peptides (Fig. 2). The His 392-containing peptide, 39 (numbered from the amino end), extends from Asn 378 to Arg 411, and has a predicted mass of 3,778, placing it in a region of the mass spectrum where unambiguous identification is expected. The Tyr 415-containing peptide, 40, extends from Leu 412 to Arg 422, and has a predicted mass of 1,331, placing it in a region of the mass spectrum with many other similar-sized peptides, complicating its identification. Peptides 39 and 40, joined through a peptide bond, would produce a peptide (39–40) of predicted mass 5,089, whereas a junction through the putative C_β-N_δ bond would give rise to a peptide (39+40) of predicted mass 5,106. These two peptides and one partial trypsin product that might contain the C_β-N_δ with mass of 5,720 are also shown in Figure 2.

The 3,000–6,000 mass range of the trypsin digest mixtures of HPII and its N201H variant are shown in Figure 3A and B, respectively. The digest mixture from the N201H variant (Fig. 3B) contains a series of fragments that are consistent with there being no linkage between fragments 39 and 40 (containing His 392 and Tyr 415, respectively). The 3,778 mass peak corresponds to fragment 39, and the 4,391 mass peak corresponds to the partial digest product composed of fragments 38 and 39. Significantly, there are no peaks at either 5,089 or 5,106 that would indicate a combination of fragments 39 and 40 either through a peptide bond not cleaved by trypsin, or the putative C_β-N_δ bond between His 392 and Tyr 415. The 3,457 mass peak varied among digests and could not be attributed to any one tryptic fragment or combination of two fragments, suggesting that it was a combination of at least three fragments.

The tryptic mixture from HPII (Fig. 3A) differed significantly from the N201H mixture in containing two peaks with masses of 5,107 and 5,721. The 5,107 mass fragment is consistent with fragments 39+40 being joined by the C_β-N_δ bond between His 392 and Tyr 415 rather than the partial tryptic product (39–40), which would have a clearly distinguishable mass of 5,089. The 5,721 mass fragment can be ascribed to the partial tryptic fragment, 38–39, joined to fragment 40 by the C_β-N_δ bond between His 392 and Tyr 415 (Fig. 2). Larger peptide products were not observed. It should also be noted that the ratio of peaks with masses of 3,778 (complete digest fragment) and 4,391 (partial digest fragment) is similar to the ratio of peaks with masses of 5,107 and 5,721.

Discussion

Novel covalent linkages and posttranslational modifications are becoming more common as protein chemistry techniques become more sensitive. The methionine sulfone found in the active site of the catalase from *P. mirabilis* (Buzy et al., 1995), the cysteine-sulfenic acid in the NADH peroxidase from *Streptococcus faecalis* (Stehle et al., 1991), the modified cysteine in catalase HPII of *E. coli* (Sevinc et al., 1995), and the internal cyclization of the peptide backbone with accompanying oxidation of the C_α-C_β bond of Tyr 66 in the green fluorescent protein (Heim et al., 1994; Ormo et al., 1996) are all recent findings. The C_β-N_δ bond joining His 392 to Tyr 415, observed now in active catalase HPII, is yet another example of a novel and unexpected linkage found deep within a protein. A diagram of the His-Tyr linkage in relation to the heme and a few other surrounding residues is shown in Figure 4. The presence of this novel bond is well supported by both the electron density of the corresponding crystal structures and the sizes of fragments in the tryptic digest maps. However, the two techniques seem to differ with respect to the proportion of HPII subunits containing the covalent C-N bond. The strong electron

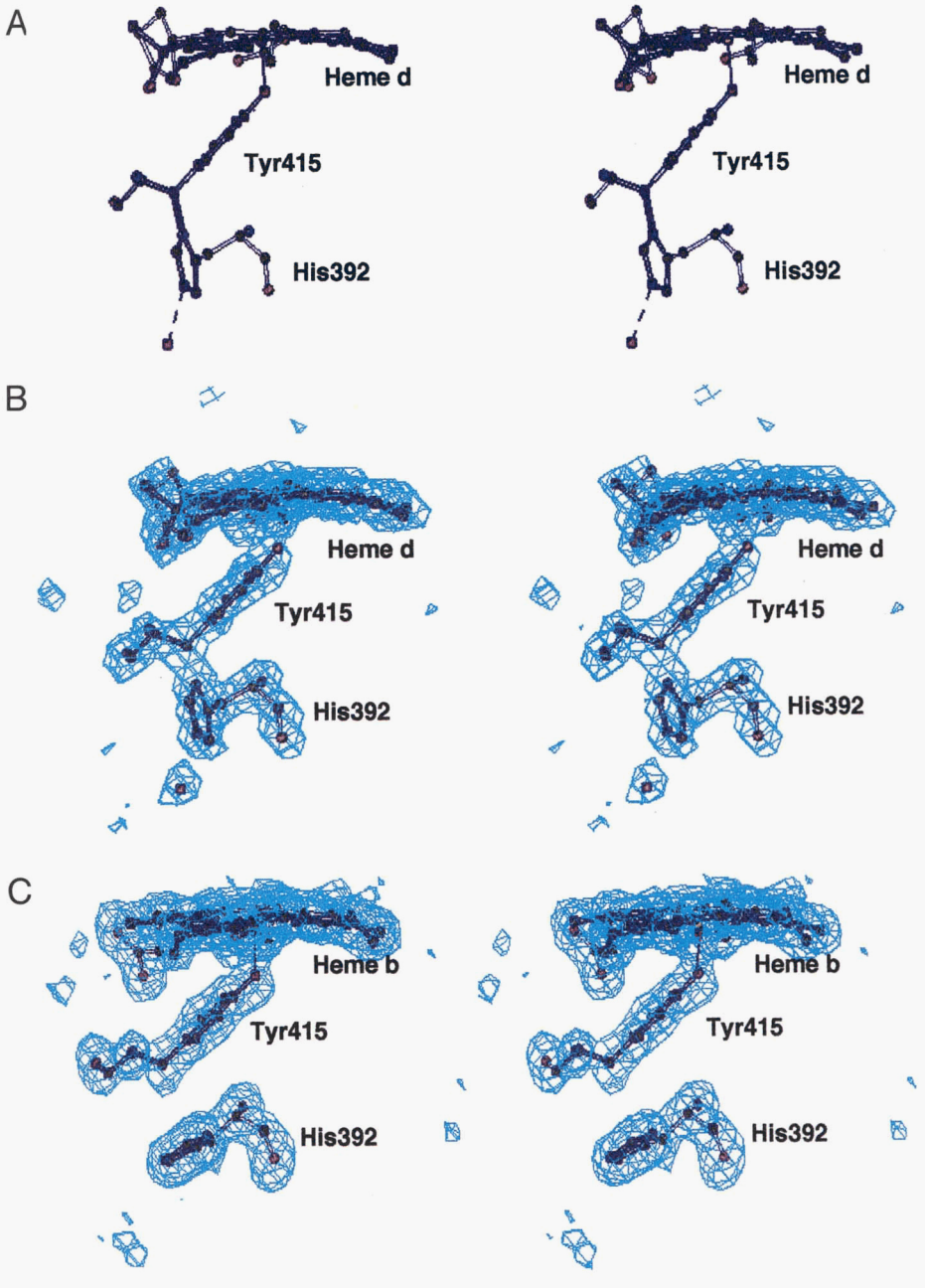

Fig. 1. Orientation of His 392 and Tyr 415 on the proximal side of the heme residue viewed from the "edge" of the tyrosine ring. **A:** Stereo view of the pocket on the proximal side of the heme in HPII showing the putative bond between C_β of Tyr 415 and N_δ of His 392. **B:** Stereo view of $(F_o - F_c)$ omit maps of the pocket on the proximal side of the heme in HPII showing the strong electron density between the C_β of Tyr 415 and N_δ of His 392. The adjacent water hydrogen bonded to the N_ϵ of His 392 is included. **C:** Stereo view of $(F_o - F_c)$ omit maps of the pocket on the proximal side of the heme *b* in the H128N variant of HPII, revealing the rotation of the imidazole ring of His 392 and the lack of strong electron density between His 392 and Tyr 415 relative to the wild-type HPII in B.

density between the imidazole of His 392 and the benzyl carbon of Tyr 415 suggests that the linkage exists in a very high proportion, close to 100%, of the subunits. In turn, the tryptic digests reveal that less than a third of the fragments containing His 392 (fragments with masses 3,778, 4,391, 5,107, and 5,721) are linked to the Tyr 415-containing fragment (fragments with mass 5,107 and 5,721). This discrepancy may indicate that the C_β-N_δ bond is relatively unstable under the conditions used for tryptic cleavage of the protein and mass determination of the digestions fragments. The ratio of complete to partially digested fragments is independent of the presence of the His-Tyr bond, consistent with an equal sensitivity of the C-N bond regardless of the completeness of the tryptic digests.

The source of the C_β-N_δ bond is a matter for conjecture at this stage. Perhaps the most significant observation, aside from the novel linkage itself, is the fact that the linkage is present only in HPII subunits where the heme *b* to heme *d* conversion (as described in Fig. 5) has also occurred. A satisfactory mechanistic

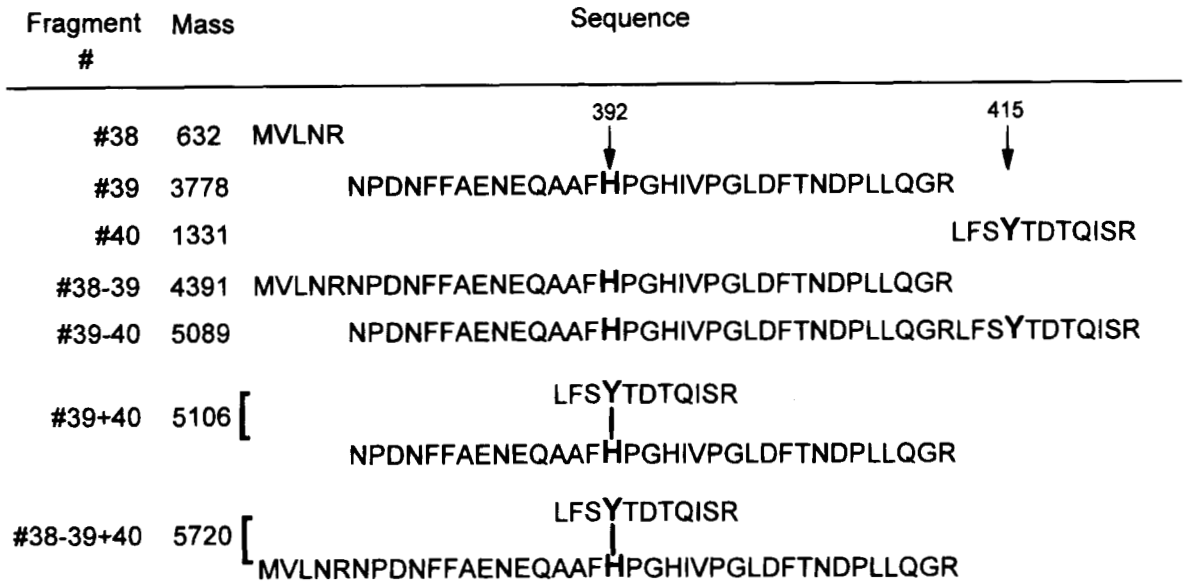

Fig. 2. Sequences and calculated masses of peptides formed on trypsin digestion of HPII. The tryptic digest fragments are numbered from the amino end and only those fragments containing or adjacent to fragments containing His 392 and Tyr 415 are shown. The sequences and calculated masses of two peptides that would arise from a linkage between His 392 and Tyr 415 are also shown. His 392 and Tyr 415 are highlighted in larger font and the linkage between them is indicated by a vertical dash between the overlapped sequences. The contribution of protonated residues are accounted for in the calculated values.

explanation for the autocatalytic heme conversion has never been proposed, but, if we assume that this reaction is linked to the His 392–Tyr 415 bond formation, we can propose the mechanism shown in Figure 6. The first part of the process that generates compound I and water in a reaction between H_2O_2 and the heme on its distal side is not shown in Figure 6, nor are the active site residues His 128 and Asn 201, required for compound I formation. Compound I, containing an oxo-Fe^{IV} moiety and a porphyrin π cation radical, is the starting point in Figure 6A. A second H_2O_2 can reach the essential Tyr 415 through the cavity on the heme proximal side to be oriented, as shown, by hydrogen bonds with one or more of the adjacent Ser 414, Thr 418, or Gln 419 residues. A concerted reaction ultimately resulting in hydroxyl addition to ring III of the heme may begin with a proton being abstracted from the N_ϵ of His 392. This would result in the N_δ of His 392 attacking the C_β of Tyr 415, displacing a hydride ion, which, in turn would attack the H_2O_2 molecule, causing the heterolytic cleavage of the O-O bond to form water and a hydroxide ion. The latter would react with the porphyrin π cation radical, producing the neutral radical shown in Figure 6B. The subsequent transfer of one electron from the heme to the oxo-iron complex would generate a cation that would facilitate the cyclization of the propionate group into the spirolactone (Fig. 6C). The net effect of this reaction sequence is that oxygen in the oxy-iron complex of compound I is converted to water, resulting in two H_2O_2 molecules (one used in the generation of compound I and one in Fig. 6A) being converted to three molecules of water and one hydroxyl group on the heme.

The formation of compound I is an obvious necessity for initiation of the mechanism, but the "trigger" of the mechanism on the proximal side is not so obvious. Extraction of the N_ϵ proton might simply involve His 395 and Asp 197, which are situated appropriately. Alternatively, an anionic species found binding to compound I of *P. mirabilis* catalase (Gouet et al., 1996), if present in HPII, might serve to extract the proton. The approximate location of such an anion in HPII (based on the *P. mirabilis* catalase structure) is shown in Figure 4, and is clearly in a location where it could accept a proton from the imidazole of His 392. The identity of the anionic species remains unknown and its presence in HPII is unconfirmed, but the fact that the anion may be present in compound I as in the *P. mirabilis* catalase provides another explanation for why inactive variants of the enzyme do not catalyze heme conversion or generate the His-Tyr linkage.

Yet another possibility is that the initial step in the mechanism depicted in Figure 6A is not a concerted process, and the initial abstraction of a hydride ion from the C_β of Tyr 415 generates an intermediate carbonium ion, stabilized by resonance with the phenyl ring, which subsequently experiences the nucleophilic attack of the N_δ of His 392. A similar oxidation, in this case carried out by atmospheric oxygen, has been proposed for the oxidation of the C_α-C_β bond of Tyr 66 in the green fluorescent protein (Cubitt et al., 1995).

In addition to coupling the two novel reactions catalyzed by HPII, the heme conversion and the C_β-N_δ bond formation, the proposed mechanism is significant in explaining how the oxidation of ring III of the heme takes place so far away from the catalytic residues His 128 and Asn 201, as shown in Figure 4. Mutation of either of these residues can prevent both the catalytic reaction and heme modification, but a rationalization of how such distantly situated residues might control the heme conversion on the opposite side of the heme was not presented. It is evident from the electron density maps that there has been no change in the main-chain positions, and only subtle changes in the side chains on the proximal side of the heme resulting from these mutations. Consequently, the lack of His-Tyr bond formation in these mutant proteins is not a result of reduced access of a necessary reactant to the region. By involving compound I formation, which requires His 128 and Asn 201, as a step in the heme oxidation, we can rationalize the involvement of these residues in heme conversion.

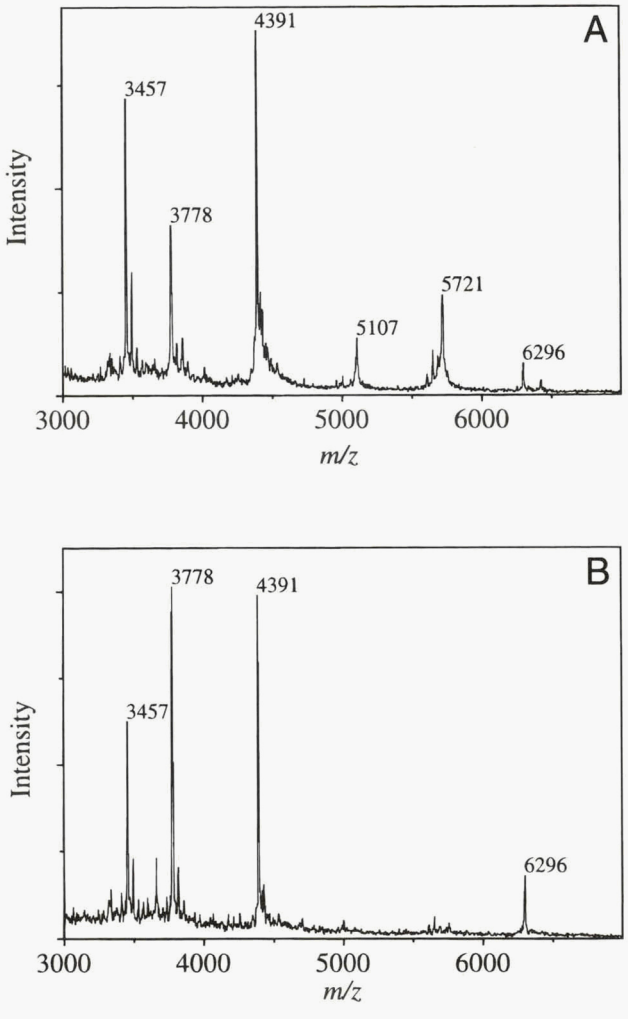

Fig. 3. Mass analysis of the mixtures of peptide fragments generated by trypsin digestion of HPII (**A**) and the N201H variant (**B**). Only the 3000–6000 mass range is shown.

Furthermore, the puzzle of how the oxidation could occur on the proximal side of the heme is explained by the involvement of a proximal-side H_2O_2 and residues immediately below ring III, as postulated in the recent report of Gouet et al. (1996).

The *P. vitale* catalase (PVC), which closely resembles HPII in size and structure, also contains the *cis*-hydroxy spirolactone heme *d* moiety, and one might logically expect the heme conversion to involve a reaction similar to HPII. However, His 392 is replaced by Glu (or Gln) (W.R. Melik-Adamyan, pers. comm.), which precludes the formation of a His-Tyr bond and calls into question the concerted mechanism in Figure 6. One possibility is that the heme conversion mechanism is different in PVC and has adapted to the absence of the imidazole ring. For example, the presence of a water molecule on the proximal side of the heme would be sufficient to explain the formation of the *cis*-hydroxy spirolactone heme *d* as shown in Figure 7. Compound I is again the starting point and the addition of a hydroxyl group from a proximal water molecule to the porphyrin cation (Fig. 7A) would lead to a radical structure depicted in Figure 7B. This intermediate would evolve in a similar fashion to the radical in Figure 6B, leading to the reduction of the oxo-iron species (Fig. 7C) and the formation of the spirolactone ring (Fig. 7D).

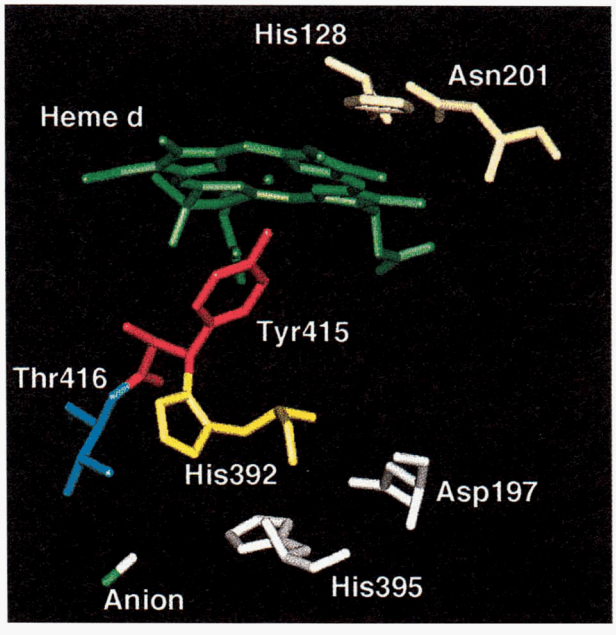

Fig. 4. Close-up view of the proximal pocket, including the C_β-N_δ bond between His 392 and Tyr 415. Residues Thr 416, Asp 197, and His 395 that might be involved directly in the His-Tyr bond formation are included in this view. The active site residues His 128 and Asn 201 are shown on the distal side of (above) the heme. The approximate location of the anion, recently found in compound I of the *P. mirabilis* catalase (Gouet et al., 1996), is also shown.

Despite the logic of coupling compound I formation to both heme modification and His-Tyr bond formation, yet another possibility is that the two modification reactions occur independently. In this event, the heme modification in both enzymes may involve the mechanism shown in Figure 7A, B, C, and D, and the His-Tyr bond formation in HPII involves reduction of hydrogen peroxide to two molecules of water, as shown in Figure 7E. An argument against this possibility is that it does not explain why inactive catalases lack the His-Tyr bond.

The possible catalytic implications of the His-Tyr bond in HPII are also an open subject. The presence of the extra linkage should

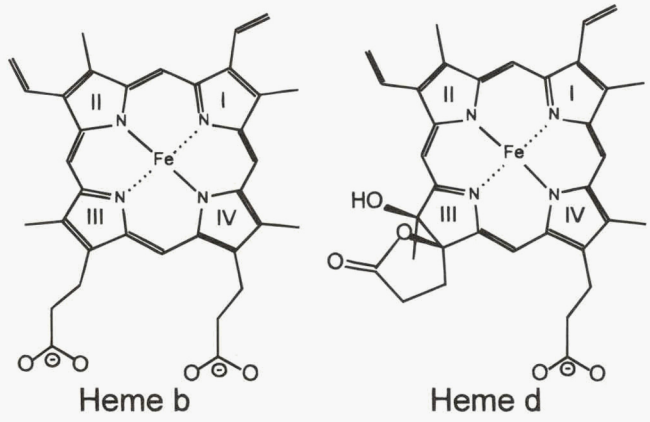

Fig. 5. Structures of heme *b* (protoheme IX) and heme *d*. The inactive variants of HPII, H128N, and N201H contain heme *b*. Wild-type HPII converts heme *b* to heme *d*.

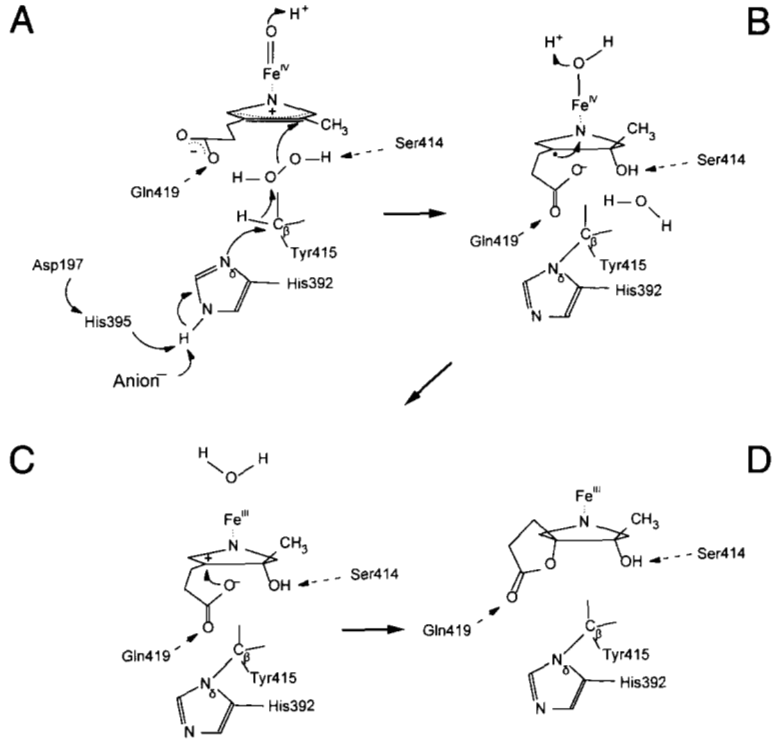

Fig. 6. A proposed mechanism coupling the formation of the His-Tyr bond to the oxidation of ring III of the heme in HPII of *E. coli*. For simplicity, the phenyl ring of Tyr 415 is not shown, and only ring III of the heme and the heme iron are shown. The mechanism begins with the formation of compound I shown in (**A**). Compound I is an oxoferryl species formed, along with water, in the reaction of one H_2O_2 with the heme. The iron is in a formal Fe^V oxidation state, but one electron is delocalized from the heme to create the oxo-Fe^{IV}-heme cation, shown as the starting species, compound I. A concerted series of reactions, possibly triggered by either Asp 197/His 395 or by a putative anionic species bound to compound I, results in the transfer of a hydroxyl to the heme from the H_2O_2 and generation of a neutral radical species in (**B**). Subsequent electron transfer from the heme to the iron would generate the cation shown in (**C**), which would facilitate spirolactone cyclization to form the final product containing the His-Tyr bond and the modified heme shown in (**D**).

introduce rigidity in the active center, and the extended structure could facilitate the movement of electrons in a larger region. Catalytic comparisons of HPII and PVC are being planned and variants of HPII that mimic the PVC proximal-side organization are now being engineered into HPII as the next stage of this study.

Materials and methods

Enzyme purification

Cultures of *E. coli* strain UM255 *pro leu rpsL hsdM hsdR endI lacY katG2 katE::*Tn*10 recA* (Mulvey et al., 1988) transformed with plasmids pAMkatE72 (von Ossowski et al., 1991), pH128N, or pN201H (Loewen et al., 1993) containing the *katE* gene or its mutant variants encoding HPII, the H128A, or the N201H variants, respectively, were grown in Luria broth containing 10 g/L tryptone, 5 g/L yeast extract, and 5 g/L NaCl. Growth of the mutant variants was for 22 h at 28 °C, and of the wild-type HPII was for 16 h at 37 °C with shaking. Cells were harvested and HPII was isolated as described previously (Loewen & Switala, 1986). DEAE cellulose (Whatman) replaced DEAE Sephadex.

Crystallization and data collection

Crystals of HPII, the H128N variant, and the N201H variant were obtained as described previously (Bravo et al., 1995). Diffraction data sets were collected using synchrotron radiation at 0.98 Å from the Synchrotron in Hamburg, Germany. Samples of catalase HPII and the variant H128N were flash frozen during data collection. Diffraction from crystals of N201H was collected at room temperature. All data sets were processed and scaled using DENZO and SCALEPACK (Otwinowski, 1993) (Table 1). Automatic refinement steps were done with the program XPLOR (Brünger, 1992) and were alternated with inspection and manual rebuilding using the graphic programs TURBO-FRODO (Rousel & Cambillau, 1994) and O (Jones et al., 1990). The corresponding final crystallographic agreement factors R and R_{free} are also indicated in Table 1.

MALDI-MS

Protein (250 μg) was boiled for 3 min in 50 mM potassium phosphate, pH 7.0, and mixed with 7 μg of trypsin at room temperature for 1 h. The solution was boiled a second time and treated with an additional 7 μg of trypsin for 1 h, after which the solution was boiled and lyophilized. The dried sample was resuspended in 2 mL of saturated α-cyano-4-hydroxycinnamic acid in acetonitrile/0.1% trifluoroacetic acid (1:2 by vol). Two microliters were applied to the sample probe and air dried for MALDI-MS using the Manitoba reflecting time-of-flight mass spectrometer (Ens et al., 1993). The instrument was operated in positive-ion linear mode. Desorption/ionization was achieved by a pulsed ultraviolet laser beam (N_2 laser, λ = 337 nm). The acceleration voltage was 30 kV and the

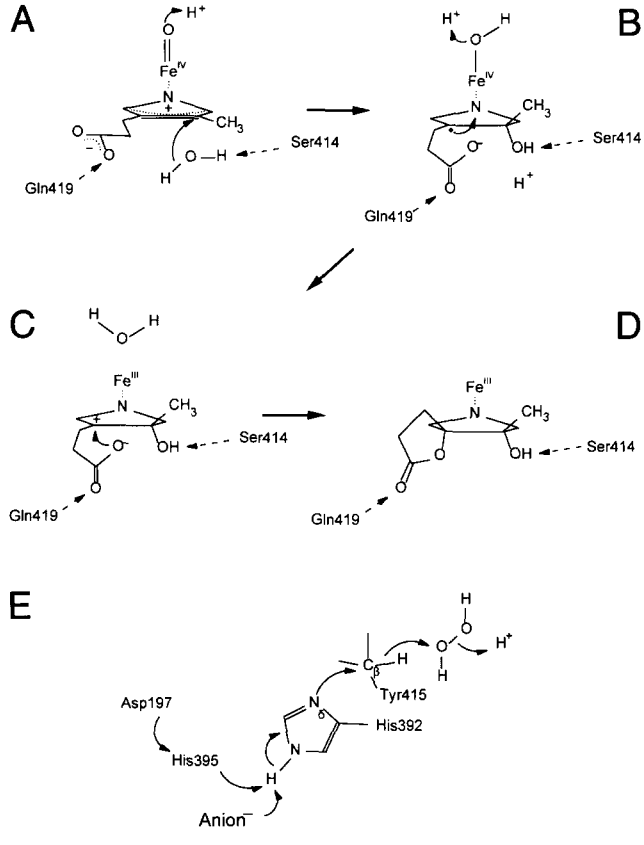

Fig. 7. An alternate mechanism to explain heme modification in the *P. vitale* catalase. A water on the proximal side of the heme is added to the heme cation species of compound I shown in (**A**) to generate a radical ion in (**B**). As in Figure 5, electron flow toward the oxo-iron would generate the cation shown in (**C**), leading to the spirolactone product shown in (**D**). In (**E**), an alternate mechanism for His-Tyr bond formation is presented that could occur independently of the heme modification reaction.

laser power density was approximately 10^6 W/cm^2. For better target uniformity, the crushed-matrix method, in which the matrix was crushed with a glass slide, was employed (Xiang & Beavis, 1994). The mass spectrum of each sample was the average of more than 100 shots. For mass calibration, insulin (5,733 Da) was used.

Acknowledgments

We thank Prof. William Melik-Adamyan for facilitating access to the refined PVC structure prior to its publication. This work was supported by an operating grant from the Natural Sciences and Engineering Research Council (NSERC) (OGP9600) to P.C.L. and a postgraduate scholarship from NSERC to A.H. Work in Barcelona was supported by grants PB92-0707 and PB95-0218 to I.F. J.B. was the recipient of a doctoral fellowship from the Generalitat de Catalunya. Data collection in Hamburg was supported by the Human Capital Mobility Project on contract CHGE-CT93-0040.

References

Bravo J, Verdaguer N, Tormo J, Betzel C, Switala J, Loewen PC, Fita I. 1995. Crystal structure of catalase HPII from *Escherichia coli*. *Structure 3*:491–502.

Brünger AT. 1992. *X-PLOR manual, version 3.1*. New Haven, Connecticut: Yale University.

Buzy A, Bracchi V, Sterjiades R, Chroboczek J, Thibault P, Gagnon J, Jouve HM, Hydry-Clergeon G. 1995. Complete amino acid sequence of *Proteus mirabilis* PR catalase. Occurrence of a methionine sulfone in the close proximity of the active site. *J Protein Chem 14*:59–72.

Cubitt AB, Heim R, Adams SR, Boyd AE, Gross LA, Tsien RY. 1995. Understanding, improving and using green fluorescent proteins. *Trends Biochem Sci 20*:448–455.

Ens W, Spicer V, Standing KG, Zhou J. 1993. Suppression of metastable interference in matrix-assisted laser desorption/ionization (MALDI) spectra in a reflecting time-of-flight mass spectrometer. *Org Mass Spectrom 28*:1430–1434.

Fita I, Silva AM, Murthy MRN, Rossmann MG. 1986. The refined structure of beef liver catalase at 2.5 Å resolution. *Acta Crystallogr B 42*:127–131.

Gouet P, Jouve HM, Dideberg O. 1995. Crystal structure of *Proteus mirabilis* catalase with and without bound NADPH. *J Mol Biol 249*:933–954.

Gouet P, Jouve HM, Williams PA, Andersson I, Andreoletti P, Nussaume L, Hajdu J. 1996. Ferryl intermediates of catalase captured by time-resolved Weissenberg crystallography and UV-VIS spectroscopy. *Nature Struct Biol 3*:951–956.

Heim R, Prasher DC, Tsien RY. 1994. Wavelength mutations and posttranslational autooxidation of green fluorescent protein. *Proc Natl Acad Sci USA 91*:12501–12504.

Jones TA, Zou JY, Cowan SW, Kjeldgaard M. 1990. Improved methods for building protein models in electron density maps. *Acta Crystallogr A 47*:110–119.

Loewen PC, Switala J. 1986. Purification and characterization of catalase HPII from *Escherichia coli* K12. *Biochem Cell Biol 64*:638–646.

Loewen PC, Switala J, von Ossowski I, Hillar A, Christie A, Tattrie B, Nicholls P. 1993. Catalase HPII of *Escherichia coli* catalyzes the conversion of protoheme to *cis*-heme *d*. *Biochemistry 32*:10159–10164.

MacGillavry CH, Rieck GD, eds. 1968. *International tables for crystallography, vol III*. Birmingham, UK: Kynoch Press.

Mulvey MR, Sorby PA, Triggs-Raine BL, Loewen PC. 1988. Cloning and physical characterization of *katE* and *katF* required for catalase HPII expression in *Escherichia coli*. *Gene 73*:337–345.

Murshudov GN, Grebenko AI, Barynin V, Dauter Z, Wilson KS, Vainshtein BK, Melik-Adamyan WR, Bravo J, Ferran JM, Ferrer JC, Switala J, Loewen PC,

Table 1. *X-ray statistics and agreement factors*

		Data collection				Refinement	
Enzyme	Temp.	R_{sym} (%)	Completeness (%)	Resolution (Å)	$I/\sigma(I)$ last shell	R-factor (%)	R_{free} (%)
HPII	100 K	8.9	98	1.9	2.5	16.0	21.1
H128N	100 K	9.6	92	1.9	3.1	14.8	21.0
N201H	Room	8.9	77	2.2	2.9	18.5	—[a]

[a]Strict noncrystallographic symmetry was maintained between the four subunits in the crystal asymmetric unit.

Fita I. 1996. Structure of the heme d of *Penicillium vitale* and *Escherichia coli* catalases. *J Biol Chem 271*:8863–8868.

Murshudov GN, Melik-Adamyan WR, Grebenko AI, Barynin V, Vagi AA, Vainshtein BK, Dauter Z, Wilson KS. 1992. Three-dimensional structure of catalase from *Micrococcus lysodeikticus* at 1.5 Å resolution. *FEBS Lett 312*:127–131.

Murthy MRN, Reid TO, Sicignano A, Tanaka N, Rossmann MG. 1981. Structure of beef liver catalase. *J Mol Biol 152*:465–499.

Ormo M, Cubitt AB, Kallio K, Gross LA, Trien RY, Remington SJ. 1996. Crystal structure of the *Aequorea victoria* green fluorescent protein. *Science 273*:1392–1395.

Otwinowski Z. 1993. Data collection and processing. In: Sawyer L, Isaacs N, Bailey S, eds. *Proceedings of the CCP4 study weekend.* Warrington, UK: SERC Laboratory. pp 56–62.

Rousel A, Cambillau C. 1994. *TURBO-FRODO manual.* Mountain View, California: Silicon Graphics Directory, Silicon Graphics.

Sevinc S, Ens W, Loewen PC. 1995. The cysteines of catalase HPII of *Escherichia coli*, including Cys438 which is blocked, do not have a catalytic role. *Eur J Biochem 230*:127–132.

Stehle T, Ahmed SA, Claiborne A, Schulz GE. 1991. Structure of NADH peroxidase from *Streptococcus faecalis* 10C1 refined at 2.16 Å resolution. *J Mol Biol 221*:1325–1344.

Vainshtein BK, Melik-Adamyan WR, Barynin V, Vagi AA, Grebenko AI. 1981. Three-dimensional structure of the enzyme catalase. *Nature 293*: 411–412.

Vainshtein BK, Melik-Adamyan WR, Barynin V, Vagi AA, Grabenko AI, Borisov V, Bartels KS, Fita I, Rossmann MG. 1986. Three dimensional structure of catalase from *Penicillium vitale* at 2.0 Å resolution. *J Mol Biol 188*:49–61.

von Ossowski I, Mulvey MR, Leco PA, Borys A, Loewen PC. 1991. Nucleotide sequence of *Escherichia coli katE*, which encodes catalase HPII. *J Bacteriol 173*:514–520.

Xiang F, Beavis RC. 1994. A method to increase contaminant tolerance in protein matrix assisted laser desorption by the fabrication of thin protein-doped polycrystalline films. *Rapid Commun Spectrom 8*:199–204.